 doi:10.20944/preprints201705.0082.v1

Article

Boundary Detection and Enhancement of Islanding Operation Investigation Under Fault Condition

Aref Pouryekta[1], Vigna K. Ramachandaramurthy [1], Sanjeevikumar Padmanaban[2,*], Lucian Mihet-Popa [3]

[1] Power Quality Research Group, Department of Electrical Power Engineering, Universiti Tenaga Nasional, 43000, Kajang, Selangor, Malaysia 1; aref.pouryekta@gmail.com (A.P.); Vigna@uniten.edu.my (V.K.R.)
[2] Department of Electrical and Electronics Engineering Science, University of Johannesburg, Auckland Park, Johannesburg 2006, South Africa
[3] Faculty of Engineering, Østfold University College, Kobberslagerstredet 5, 1671 Kråkeroy; Building: S 316, Norway; lucian.mihet@hiof.no
* Correspondence: sanjeevi_12@yahoo.co.in; Tel.: +27-79-219-9845.

Abstract: Distribution systems can form islands when faults occur. Each island represents a subsection with variable boundaries subject to the location of a fault(s) in the system. A subsection with variable boundaries is referred to as island in this paper. For operation in autonomous mode, it is imperative to detect the island configurations and stabilize these subsections. This paper presents a novel scheme for the detection of islanding boundaries and stabilizing the system during autonomous operation. In the first stage, a boundary detection method is proposed to detect the configuration of the island. In the second stage a dynamic voltage sensitivity factor (DVSF) is proposed to assess the dynamic performance of the system. In the third stage, a wide area load shedding program is adopted based on DVSF to shed the load in weak busbars and stabilize the system. The proposed scheme is validated and tested on a generic 18-bus system using a combination of EMTDC/PSCAD and MATLAB softwares.

Keywords: islanding 1; load management 2; power distribution 3; voltage fluctuations 4

1. Introduction

The introduction should briefly place the study in a broad context and highlight why it is important. It should define the purpose of the work and its significance. The current state of the research field should be reviewed carefully and key publications cited. Please highlight controversial and diverging hypotheses when necessary. Finally, briefly mention the main aim of the work and highlight the principal conclusions. As far as possible, please keep the introduction comprehensible to scientists outside your particular field of research. References should be numbered in order of appearance and indicated by a numeral or numerals in square brackets, e.g., [1] or [2,3], or [4–6]. See the end of the document for further details on references.

In recent decades, environmental concerns about greenhouse gases and global warming caused by fossil fuels have attracted many countries to adopt renewable energy sources (RES). RES based microgrids are new structures in modern electrical distribution networks. Predefined clusters of dispersed generator (DG) units associated with their vicinity loads provide the opportunity to form a microgrid (MG), which functions as a subsystem in the distribution network. Two operation modes can be defined for microgrids: grid connected mode and autonomous mode. In a grid-connected mode, MGs are able to exchange the energy with the upstream network. For the autonomous mode, during a grid failure or islanding, MG assures continues power supply to local loads and increases system reliability.

Electrical connections between unspecified number of busbars and main grid can be lost due to faults in the electrical distribution system. Hence, provided that at least one DG unit remains in the separated section, an active island can be formed. Based on IEEE-Standard 1547, islanding should be

Preprints (www.preprints.org) | NOT PEER-REVIEWED | Posted: 9 May 2017 doi:10.20944/preprints201705.0082.v1

detected and DG units must cease to supply within 2 seconds. Due to the high penetration of RES in distribution systems, islanded operation mode for DG units are considered by many utility providers as a suitable approach to maintain continuity and reliability of supply. However, as faults can occur at any point in a distribution system, the configuration of the active subsections formed is unpredictable. Hence, a subsection with non-fixed boundaries is referred to as an island. A schematic diagram of a distribution network with MG and islands is shown in Figure 1. There are several possibilities to form islands via opening breakers BK1-BK37. The identification of the island configuration is one of the important requirements for the power system analysis. Moreover, in order to stabilize the system and to conduct a voltage stability study, it is important to detect new system configuration(s) immediately after removing the faulty section. Furthermore, the new topology of the system is vital for triggering the self-healing scenarios such as load shedding and system reconfiguration.

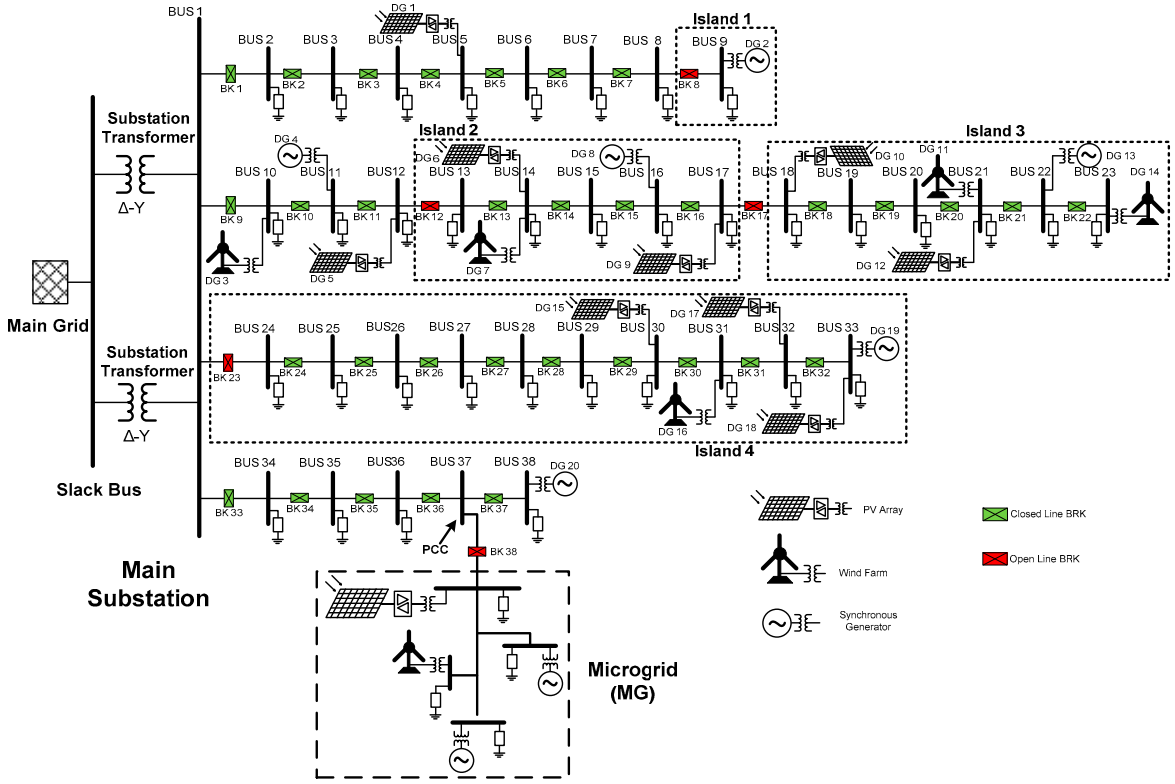

Figure 1. Single line diagram of a RES base integrated distribution network include MG and islands.

Once islanding takes place, if the generation does not meet the load demand, load shedding is unavoidable to prevent voltage collapse. In order to enhance the voltage stability of the island, less stable busbars can be chosen for load shedding. Thus, different voltage stability indices (VSI) can be used based on the system characteristics to determine weak busbars in the system. VSIs indicate the stability status of the busbars and line sections. When islanding takes place in the system, an online voltage stability index can be utilized based on the new system structure results to determine the weakest busbars for load shedding.

In order to detect islanding, three islanding detection methods (IDMs) have been developed; Active Detection Method (ADM), Passive Detection Method (PDM) and Remote Detection Method (RDM). The philosophy of the PDM is to measure the variables at PCC and compare with the reference values to detect the islanding. The advantages of these methods include simplicity and low cost to implement as they use conventional metering and protection devices to detect islanding. The characteristic of some PDMs are presented and compared in Table (1).

Preprints (www.preprints.org) | NOT PEER-REVIEWED | Posted: 9 May 2017 doi:10.20944/preprints201705.0082.v1

Table (1): Comparison between the passive islanding detection methods.

Method	Feature of each method				Advantage & disadvantages	Reference
	Run-on Time	NDZ	Error rate	Power quality		
Over/UnderVoltage And Frequency	Within 2 s	Large	Low	No impact	Easy to implement but speed is unpredictable.	[1-9]
ROCOF	24 ms	Small	High	No impact	Even in balance condition, any disturbance can result in mis-detection of islanding. Hard to choose threshold. Sensitive to load switching and fluctuation.	[10, 11]
ROCOF Over Power	100 ms	Smaller	Low	No impact	It can detect islanding effectively when power imbalance is small.	[11]
ROCOP	24–26 ms	Small	High	No impact	Its detection speed is not affected when the power mismatch between DG and load is small. It is able to quickly detect unsynchronized reclosing of the utility.	[10, 11]
Phase Jump Detection	10–20 ms	Large	Low	No impact	Difficult to implement and select threshold. Uses PLL to control.	[5,11] [17]

The performance of ADM is based on perturbation and observation concept. A DG parameter is chosen to be distorted by injecting perturbation. In stiff grid, the amplitude of the variations at DG unit terminal are negligible since the grid parameters are dominant. However, injecting disturbance into the terminal result in significant variation on DG parameters during the islanding phenomenon. Table (2) presents the characteristics of different ADMs.

Table (2): Comparison between Active Detection Methods.

Method	Feature of each method				DG Type	Advantage & disadvantages	Reference
	Time	NDZ	Error rate	Power quality			
Impedance Measurement	0.77 s - 0.95 s	Very Small	Low	Degrade	SG	Low performance in presence of multiple DG units. Introduce harmonic. Hard to adjust the thresholds. Injection of sub-harmonics into inverter output.	[12, 13] [10, 14, 15]
Active Frequency Drift (AFD)	< 2s	Large for high *Qf*	High	Degrade	VSC	NDZ is decreased as well as error ratio. Low performance in presence of multiple dg. Sensitive to the load. Unable to detect for unity PF.	[16, 17] [1, 10, 18]
Frequency Jump (FJ)	75 ms	Small (Less than AFD)	Low	Slightly degrade	VSC	Low performance in presence of multiple DG units.	[10]
Negative Sequence Voltage Injection	60 ms-120 ms	Non		Degrade	VSC	High performance in presence of multiple DG unit	[15, 19-21]
Negative Sequence Current Injection Method	60 ms	Non	Low	Degrade	VSC	Not sensitive to load change. The accuracy is higher than detecting positive-sequence voltage. High performance in presence of multiple DG unit.	[10, 11, 20-22]

Remote detection methods are developed to overcome the problems faced by existing methods. The RDMs employ a communication pattern between DG unit and main grid to alert and disconnect

Preprints (www.preprints.org) | NOT PEER-REVIEWED | Posted: 9 May 2017 doi:10.20944/preprints201705.0082.v1

the DG units once unintentional islanding occurred. Remote Detection Methods are applicable to the systems with multiple DG units which includes both inverter based sources and synchronous generators. The Remote Detection Methods are presented in Table (3).

In [23-29], different load shedding methods have been developed for microgrids. Measurement of the system parameters such as voltages, frequency and rate of change of frequency reveals the imbalance between generation and load demand. Hence, the load shedding method would assure the stable operation. However, not all these methods are able to do the load shedding for the islands since the busbars for load shedding cannot be predefined.

Table (3): Comparison between Remote Detection Methods.

Method	Feature of each method				Advantage & Disadvantages	Ref.
	Time	NDZ	Error rate	Power quality		
Supervisory control and data acquisition (SCADA)	Depend on the system	None	None	No impact	This method provides more control signal to control DG units. Detection speed depend on the system characteristics.	[10, 16, 30, 31]
Power Line Carrier Signaling (PLCS)	200 ms	None	None	Very Small Impact	PLCS is applicable for both DG types. Uses existing electrical network as a path for signaling. Suitable for large networks with high penetration of DG units since it is costly.	[10, 32-34]
Signal Produced By Disconnect (SPD)	100 ms-300 ms	None	None	No impact	Needs large investment to establish a communication network.	[10, 15, 35]

Since these IDMs monitor voltage, current etc. at the point of common coupling (PCC), they can detect the islanding of DG Units. However, these methods are not capable of identifying the boundary of the island. The proposed method here is able to detect the boundary of the island and determine the available generation and load in each island. Moreover, the proposed method can be applied on meshed network. As well as the proposed method is applicable for the systems with non-consecutive busbar numbering.

In order to determine the system voltage stability status, various indices have been developed [36-38]. Voltage stability analysis can be categorized as dynamic analysis and static analysis uses static voltage stability indices (SVSI). Pre-islanding information or microgrid information is used to assess the voltage stability of the system using SVSIs. Hence, SVSIs do not reflect the dynamic operation of the power system during contingencies. However, dynamic analysis identifies the system parameters during transient and steady state conditions. Thus, an index is required to identify dynamic performance and system stability.

Modified graph theory is utilized to detect the boundary of each island. In the second step, in order to perform a wide area load shedding, a dynamic voltage sensitivity factor (DVSF) is proposed to specify the weak busbars in the system. The proposed DVSF shows the relevancy of reactive power and voltage at each busbar. Thus, the most sensitive busbars based on new configuration of the system are chosen for load shedding.

This paper is organized as follows: Section (2) explains the methodology of the proposed algorithm. Section (3) presents the boundary detection method for islands. Section (4) elaborates the calculation of dynamic sensitivity factor for the islands. In section (5), a practical test network is

Preprints (www.preprints.org) | NOT PEER-REVIEWED | Posted: 9 May 2017 doi:10.20944/preprints201705.0082.v1

utilized to validate the proposed scheme. Simulation results are investigated in section (6) and the conclusion is presented in section (7).

2. Proposed Scheme to Stabilize the System

This section may be divided by subheadings. It should provide a concise and precise description of the experimental results, their interpretation as well as the experimental conclusions that can be drawn. The proposed scheme assumes that voltage and current measurements are available at each busbar. When islanding occurs in the system, the number of islands is identified using the proposed detection method. The proposed algorithm also specifies the busbars belonging to each island. The main idea of this method is to determine the configuration of the islands and maintain system stability. When island configuration is determined, the amount of available generation and load demand are disclosed. Load shedding in the weakest busbar prevents voltage collapse in the system. Weak busbars are chosen based on the dynamic voltage sensitivity factor. In order to conform to IEEE-1547 standard, after the first round of load shedding, if the system frequency division exceeds the ±1% of its rating, further load shedding will be done at the next weak busbar based on the new DVSF. This procedure is repeated until a stable operation point for all Islands is gained. A flowchart of the proposed algorithm is depicted in Figure 2.

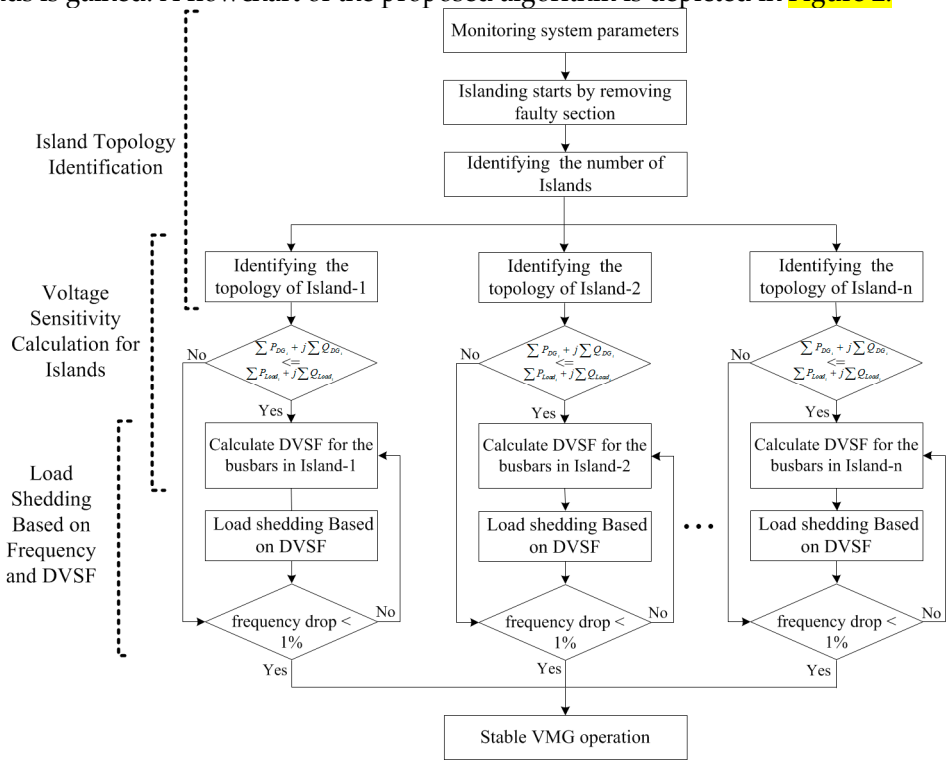

Figure 2. Flowchart of the proposed scheme to stabilize a system after islanding

3. Boundary Detection Using Graph Model

The focus of existing detection methods is to detect the islanding at PCC. However, in this paper, a boundary detection algorithm based on modified graph theory is proposed to identify the islands topology once they are formed. A simplified graph theory is utilized for different purposes such as microgrid reconfiguration [39] and load flow calculation [40].

3.1. Node Integration Matrix

In this section, mathematical model of the proposed boundary detection method is presented. For this purpose, a graph consisting of 10 edges and 8 vertices with three subsections is considered. The graph is shown in Figure 3. As a first step, all the vertices should be numbered. Numbering of the vertices is random and each vertex should get a number. In the second step, connections between

Preprints (www.preprints.org) | NOT PEER-REVIEWED | Posted: 9 May 2017 doi:10.20944/preprints201705.0082.v1

each vertex were investigated. In order to determine all connections in this graph, a node integration matrix $[NIM]_{n,n}$ where n represents the number of vertices is defined as follows:

$$\begin{cases} NIM_{i,j} = 1 & \text{If there is a connection between } i \text{ and } j \\ NIM_{i.j} = 0 & \text{If there is no connection between } i \text{ and } j \\ NIM_{i,i} = 1 \end{cases}$$

If there is a connection between two vertices, the related elements will be unity. The value 0 indicates no connection between two vertices. Moreover, in this matrix, the diagonal elements are assumed to be 1, since the proposed search algorithm will use these particular numbers and copies them in [TMC] matrix. Equation (1) represents the [*NIM*] for the graph of Figure 3.

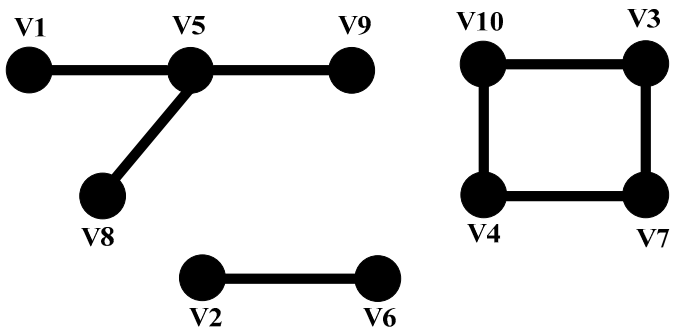

Figure 3. A graph consisting of 10 edges and 8 vertices with non-consecutive numbering.

This matrix represents the existence of edges between vertices of the graph. However, the topology of the subsections still should be extracted from this matrix.

$$[NIM] = \begin{bmatrix} 1 & 0 & 0 & 0 & 1 & 0 & 0 & 0 & 0 & 0 \\ 0 & 1 & 0 & 0 & 0 & 1 & 0 & 0 & 0 & 0 \\ 0 & 0 & 1 & 0 & 0 & 0 & 1 & 0 & 0 & 1 \\ 0 & 0 & 0 & 1 & 0 & 0 & 1 & 0 & 0 & 1 \\ 1 & 0 & 0 & 0 & 1 & 0 & 0 & 1 & 1 & 0 \\ 0 & 1 & 0 & 0 & 0 & 1 & 0 & 0 & 0 & 0 \\ 0 & 0 & 1 & 1 & 0 & 0 & 1 & 0 & 0 & 0 \\ 0 & 0 & 0 & 0 & 1 & 0 & 0 & 1 & 0 & 0 \\ 0 & 0 & 0 & 0 & 1 & 0 & 0 & 0 & 1 & 0 \\ 0 & 0 & 1 & 1 & 0 & 0 & 0 & 0 & 0 & 1 \end{bmatrix} \quad (1)$$

3.2. Topology Connection Matrix

Once the node integration matrix is calculated, the topology Connection Matrix $[TCM]_{n,n}$ is carried out. The topology connection matrix represents the subsections and the vertices in each subsection. Similar to the node integration matrix, [*TCM*] is a square matrix and the number of rows and columns depends on the number of vertices. The [*NIM*] is utilized to determine all routes in the system. The steps of determining the subsection is as follow:

Preprints (www.preprints.org) | NOT PEER-REVIEWED | Posted: 9 May 2017 doi:10.20944/preprints201705.0082.v1

a) As a first step, vertex V1 is chosen and the route starting from this vertex to other vertices is determined. for this purpose, existence of any edge between V2 and V1 is investigated. If any connection is found between V2 and V1, then connection between V3 and V2 will be checked and this will continue for the next vertex. Using this method, the route starts from V1 can be determined.

b) In the second step, since there is a possibility of more than one edge connected to V1, the connection between other unchecked vertices and V1 should be investigated. This step is repeated to find a link between all other vertices and V1.

The same steps are applied to the rest of the vertices to determine all the subsections. In Figure 4, the flowchart for calculating the [*TCM*] is depicted. According to this flowchart, the following are the steps to determine the island's boundary:

1) For a graph with n vertices, an identity square matrix is formed.
2) Start to build the ith row.
3) If $NIM_{j,k}$=1, there is a connection between jth vertex and upstream kth vertices. Then, set the $TCM_{i,j} = TCM_{i,k}$.
4) Repeat the procedure from step (2) to build the next row of [*TCM*] for all the vertices.

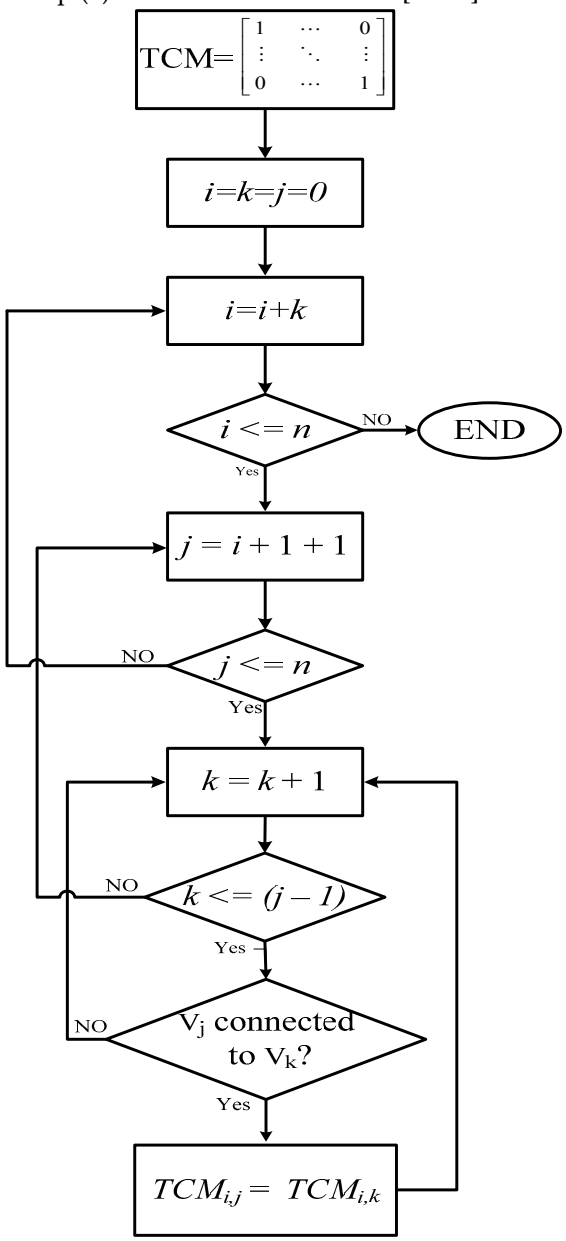

Figure 4. [*TCM*] calculation flowchart

Preprints (www.preprints.org) | NOT PEER-REVIEWED | Posted: 9 May 2017 doi:10.20944/preprints201705.0082.v1

Since the connection between one vertex to other vertices is checked just once by this algorithm, time will be saved. Moreover, since all the routes are determined using the above procedures, this algorithm can be applied on graphs with loops as well. Equation (2) represents the [*TCM*] matrix for the graph of Figure 3. When a consecutive numbering for vertices is used, The [TMC] can be calculated using Equation (2).

$$[TCM]=\begin{bmatrix}1&0&0&0&1&0&0&1&1&0\\0&1&0&0&0&1&0&0&0&0\\0&0&1&1&0&0&1&0&0&1\\0&0&1&1&0&0&1&0&0&1\\1&0&0&0&1&0&0&1&1&0\\0&1&0&0&0&1&0&0&0&0\\0&0&1&1&0&0&1&0&0&1\\1&0&0&0&1&0&0&1&1&0\\1&0&0&0&1&0&0&1&1&0\\0&0&1&1&0&0&1&0&0&1\end{bmatrix} \quad (2)$$

3.3. Boundary Detection Matrix

In the previous section, the topology connection matrix is formed and the subsections are marked. In this step, vertices in each subsection are extracted and Boundary Detection Matrix $[BDM]_{n_s,n_v}$ is formed. In this matrix, n_s represents the number of subsections and n_v represents the number of vertices in the largest subsection. The maximum n_s is equal to n when all the vertices are separated and no edge in the graph. In contrast, the maximum value for n_v is obtained for integrated graphs without any subsection. As shown in Equation (2), each row indicates one subsection.

The steps for extracting the vertices and determining the boundary of each subsection are as follow:

a) First, in the first row of [*TCM*], the column numbers of those elements that are equal to 1 are taken to the [*BDM*].
b) Second, when column numbers (for example: column 1 and column 2) has been taken to [*BDM*], all the elements in the in the [*TCM*] rows with same number (row 1 and row2) have been changed to 0.
c) Third, the next row with non-zero elements is checked with the same procedure that explained in (a).

When the entire rows of the [*TCM*] are checked, the [*BDM*] matrix will be completed. The flowchart to identify the subsections and vertices in each section is depicted in Figure 5. The following are the steps to calculate [*BDM*]:

1) Start with m^{th} row of [*TMC*] to find if there is 1 in this row.
2) Set the $BDM_{i,j}$ to m (i^{th} is based on number of subsections).
3) Set entire m^{th} row of [*TMC*] to zero and go to step 1.

Equation (3) shows the [*BDM*] matrix calculated using the procedures mentioned previously. Three different subsections including the number of vertices in each section are shown using Equation (3). One important advantage of the proposed method is the ability to detect the boundaries in meshed networks with various loops and non-consecutive busbar numbering.

$$[BDM]=\begin{bmatrix}1&2&3&4&5\\6&7&8&9&0\\10&11&12&0&0\end{bmatrix} \quad (3)$$

Preprints (www.preprints.org) | NOT PEER-REVIEWED | Posted: 9 May 2017 doi:10.20944/preprints201705.0082.v1

4. Dynamic Voltage Sensitivity

In this paper, a novel dynamic voltage sensitivity factor is proposed to provide useful information about the system's dynamic performance during islanding. Online calculation of instantaneous static voltage stability provides a pattern of points, which can be used as a dynamic

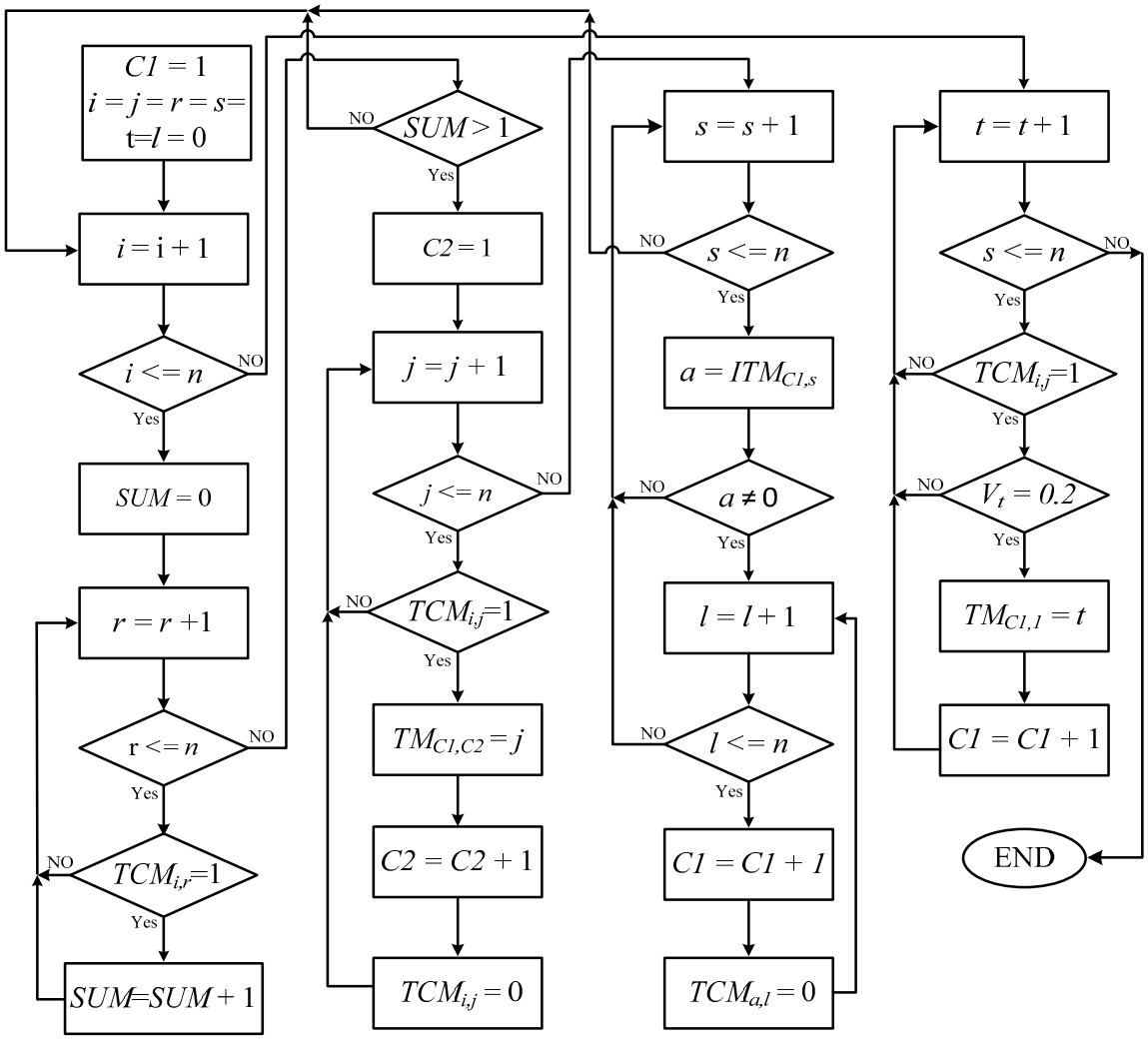

Figure 5. Procedure to extract subsections and busbars

index to determine the system voltage stability for each busbar. The DVSF reflects the influence of changes in system parameters on each busbar's stability status and determines the weak busbar before and after islanding. Conventional load flow *Jacobian* matrix is used to determine the DVSF. In order to calculate the DVSF, busbar admittance matrix [Y_{bus}] and *Jacobian* matrix is re-calculated based on the system configuration. A three-dimension [Y_{bus}] is defined according to the new configuration of the system. Figure 6 demonstrates the [Y_{bus}] for a system with n_s islands. The size of the new [Y_{bus}] is (n_v,n_v,n_s). In this matrix, m^{th} layer represents the calculated elements for m^{th} island.

Preprints (www.preprints.org) | NOT PEER-REVIEWED | Posted: 9 May 2017 doi:10.20944/preprints201705.0082.v1

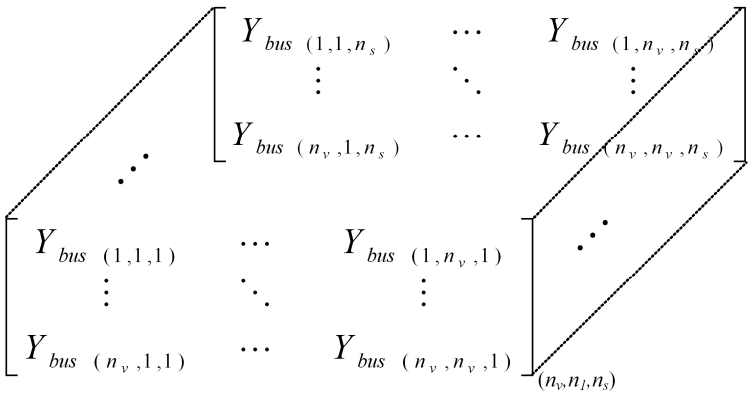

Figure 6. Three-dimensional admittance matrix

Similarly, a new *Jacobian* matrix according to the new system configuration is calculated. The dimensions of the new *Jacobian* matrix are $(2n_v \times 2n_v \times n_s)$. Equations (4-8) represents the m^{th} layer of the *Jacobian* matrix calculated for the m^{th} island in the system.

$$[J]^{(m)} = \begin{bmatrix} J_1^m & | & J_2^m \\ -- & -- & -- \\ J_3^m & | & J_4^m \end{bmatrix} \tag{4}$$

$$J_1^m = \begin{cases} \dfrac{\partial P_{i,m}}{\partial \delta_{i,m}} = \sum_{j \neq i} |V_{i,m}||V_{j,m}||Y_{i,j,m}| \sin\left(\theta_{i,j,m} - \delta_{i,m} + \delta_{j,m}\right) \\ \dfrac{\partial P_{i,m}}{\partial \delta_{j,m}} = -|V_{i,m}||V_{j,m}||Y_{i,j,m}| \sin\left(\theta_{i,j,m} - \delta_{i,m} + \delta_{j,m}\right) \forall j \neq i \end{cases} \tag{5}$$

$$J_2^m = \begin{cases} \dfrac{\partial P_{i,m}}{\partial |V_{i,m}|} = 2|V_{i,m}||Y_{i,i,m}| \cos\left(\theta_{i,j,m} - \delta_{i,m} + \delta_{j,m}\right) + \sum_{j \neq i} |V_{j,m}||Y_{i,j,m}| \cos\left(\theta_{i,j,m} - \delta_{i,m} + \delta_{j,m}\right) \\ \dfrac{\partial P_{i,m}}{\partial |V_{j,m}|} = |V_{i,m}||Y_{i,j,m}| \cos\left(\theta_{i,j,m} - \delta_{i,m} + \delta_{j,m}\right) \forall j \neq i \end{cases} \tag{6}$$

$$J_3^m = \begin{cases} \dfrac{\partial Q_{i,m}}{\partial \delta_{i,m}} = \sum_{j \neq i} |V_{i,m}||V_{j,m}||Y_{i,j,m}| \cos\left(\theta_{i,j,m} - \delta_{i,m} + \delta_{j,m}\right) \\ \dfrac{\partial Q_{i,m}}{\partial \delta_{j,m}} = -|V_{i,m}||V_{j,m}||Y_{i,j,m}| \cos\left(\theta_{i,j,m} - \delta_{i,m} + \delta_{j,m}\right) \forall j \neq i \end{cases} \tag{7}$$

$$J_4^m = \begin{cases} \dfrac{\partial Q_{i,m}}{\partial |V_{i,m}|} = -2|V_{i,m}||Y_{i,i,m}| \sin\left(\theta_{i,j,m} - \delta_{i,m} + \delta_{j,m}\right) - \sum_{j \neq i} |V_{j,m}||Y_{i,j,m}| \cos\left(\theta_{i,j,m} - \delta_{i,m} + \delta_{j,m}\right) \\ \dfrac{\partial Q_{i,m}}{\partial |V_{j,m}|} = -|V_{i,m}||Y_{i,j,m}| \sin\left(\theta_{i,j,m} - \delta_{i,m} + \delta_{j,m}\right) \forall j \neq i \end{cases} \tag{8}$$

Accordingly, Equation (9) represents the relation between reactive power and the voltage for all the busbars in islands when active power exchange is assumed to be zero ($\Delta P = 0$).

$$[\Delta Q]_{n_v,1,n_s} = [J_R]_{n_v,n_v,n_s} [\Delta V]_{n_v,1,n_s} \tag{9}$$

Preprints (www.preprints.org) | NOT PEER-REVIEWED | Posted: 9 May 2017 doi:10.20944/preprints201705.0082.v1

Equation (10) represents the reduced matrix calculated for the m^{th} island in the system. In this Equation, $[J_R]^{(m)}$ is known as a reduced *Jacobian* matrix of the m^{th} island in the system.

$$[J_R]^{(m)} = \left[J_4^{(m)} - J_3^{(m)} J_1^{-1(m)} J_2^{(m)}\right] \tag{10}$$

Change in voltage with regards to the injected reactive power for the m^{th} island can be defined by Equation (11).

$$[\Delta V]^{(m)} = \left[J_R^{-1}\right]^{(m)} [\Delta Q]^{(m)} \tag{11}$$

Diagonal values of the $[J_R^{-1}]^{(m)}$, represents the voltage sensitivity for each busbar of the m^{th} island in the system. DVSF is defined individually for each busbar. Positive and small values for DVSF indicate stable operation. On the contrary, high values for sensitivity factor are obtained when the system is near its stability margins. Negative values represent unstable operation and very small negative values represent very unstable operation. Since the relation between voltage and reactive power is nonlinear, the magnitude of the sensitivity factor in different operating conditions does not provide the degree of the stability [41].

5. Generic Test Distribution System

A modified 11 kV, 50 Hz generic network from a Malaysian electrical distribution utility was modeled using EMTDC/PSCAD in order to investigate the proposed boundary detection method and dynamic voltage sensitivity factor. The single line diagram of this network is presented in Figure 7. The network has 18 busbars and 17 overhead lines. Both transformers in the main substation are 132/11 kV, Δ-Y_g, rated at 30 MVA and impedance 10%. Fault level at 132 kV busbar is 14 kA and at 11 kV is 17.8 kA. Three 2 MVA synchronous generators were used as DG units as shown in Figure 7. The DG units are equipped with droop control to adjust the voltage and frequency after islanding. Each generator is connected to the distribution network via 0.4/11 kV, 3 MVA Y_g-Y_g transformer with 5% impedance. Simulation results are discussed in detail in the next section.

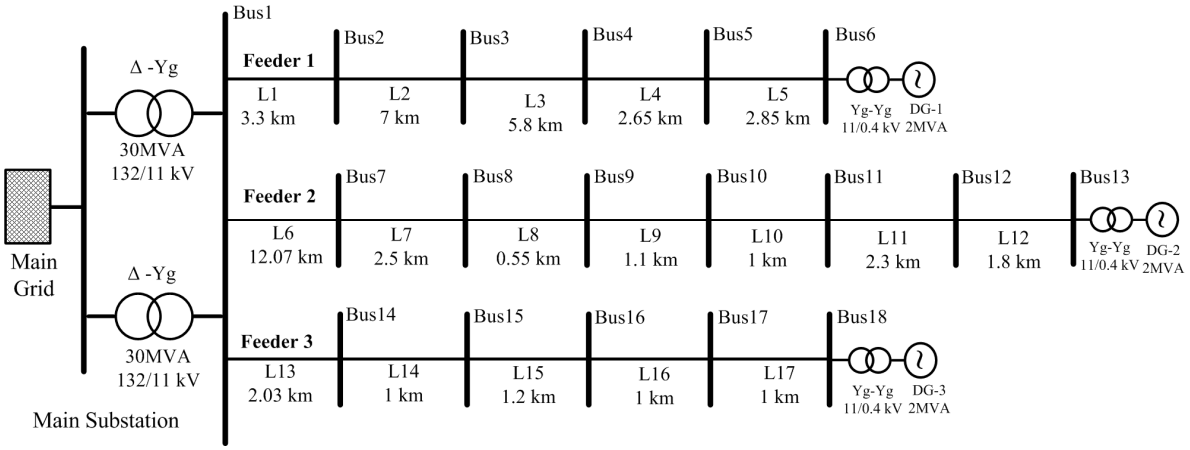

Figure 7. A single line diagram for a practical 18-busbar distribution network

6. Results and Discussion

A case study with three islands was investigated to verify the performance of the proposed methods. In order to model the system, PSCAD/EMTDC and MATLAB were utilized. The network was modeled in PSCAD and the proposed algorithms were analyzed in MATLAB. A user defined block was used as an interface to exchange the data between the softwares and to send the wide area load shedding commands from MATLAB to PSCAD. Synchronous generator 'start event' was

Preprints (www.preprints.org) | NOT PEER-REVIEWED | Posted: 9 May 2017 doi:10.20944/preprints201705.0082.v1

simulated via releasing the rotor at 2 sec. Intentional islanding was initiated in the system after 15 seconds via opening the line sections L1, L9 and L13 as in Figure 7. The opening of three line sections split the network to four subsystems. In the first step, results for the island boundary detection method were investigated. In the second step, DVSFs were shown for one island. In the third step, the wide area load shedding results based on dynamic voltage sensitivity factor were presented.

6.1. Island Boundary Detection Results

The equivalent graph for the given test system is shown in Figure 8. It was assumed that the voltage and current measurements were available in each busbar. After the tie line breakers opened, current would be reduced to zero in that line section. Hence, all downstream busbars were considered as an island, provided that a source existed. As explained in section (II), the node integration matrix $[NIM]_{18\times18}$ was calculated as follows:

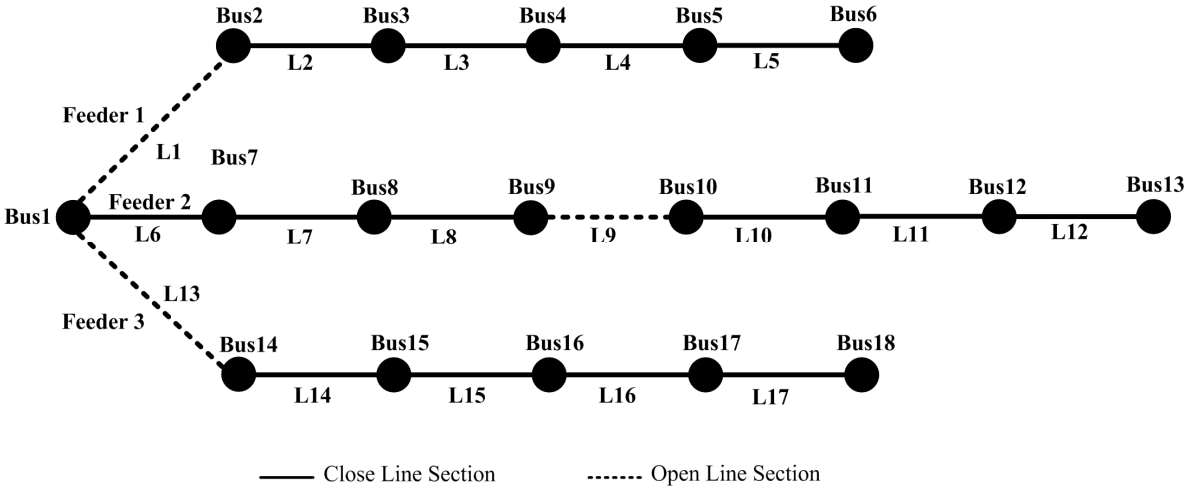

Figure 8. Equivalent graph for the test system with four subsections

$$[NIM]=\begin{bmatrix}
1&0&0&0&0&0&1&0&0&0&0&0&0&0&0&0&0&0\\
0&1&1&0&0&0&0&0&0&0&0&0&0&0&0&0&0&0\\
0&1&1&1&0&0&0&0&0&0&0&0&0&0&0&0&0&0\\
0&0&1&1&1&0&0&0&0&0&0&0&0&0&0&0&0&0\\
0&0&0&1&1&1&0&0&0&0&0&0&0&0&0&0&0&0\\
0&0&0&0&1&1&0&0&0&0&0&0&0&0&0&0&0&0\\
1&0&0&0&0&0&1&1&0&0&0&0&0&0&0&0&0&0\\
0&0&0&0&0&0&0&1&1&0&0&0&0&0&0&0&0&0\\
0&0&0&0&0&0&0&1&1&0&0&0&0&0&0&0&0&0\\
0&0&0&0&0&0&0&0&0&1&1&0&0&0&0&0&0&0\\
0&0&0&0&0&0&0&0&0&1&1&1&0&0&0&0&0&0\\
0&0&0&0&0&0&0&0&0&0&1&1&1&0&0&0&0&0\\
0&0&0&0&0&0&0&0&0&0&0&1&1&0&0&0&0&0\\
0&0&0&0&0&0&0&0&0&0&0&0&0&1&1&0&0&0\\
0&0&0&0&0&0&0&0&0&0&0&0&0&1&1&1&0&0\\
0&0&0&0&0&0&0&0&0&0&0&0&0&0&1&1&1&0\\
0&0&0&0&0&0&0&0&0&0&0&0&0&0&0&1&1&1\\
0&0&0&0&0&0&0&0&0&0&0&0&0&0&0&0&1&1
\end{bmatrix} \quad (12)$$

In order to form the node integration matrix [*NIM*], the system topology was monitored using current measurements. The line section with none zero current was considered as a closed line. Using the procedure explained in section (2), the calculated $[TCM]_{18\times18}$ is shown in Equation (13) for the test distribution network. To extract the number of busbars and corresponding Islands, the

Preprints (www.preprints.org) | NOT PEER-REVIEWED | Posted: 9 May 2017 doi:10.20944/preprints201705.0082.v1

procedure, which is depicted in Figure 5, was applied on the calculated topology connection matrix. The calculated

$$[TCM]=\begin{bmatrix}
1&0&0&0&0&0&1&1&1&0&0&0&0&0&0&0&0&0\\
0&1&1&1&1&1&0&0&0&0&0&0&0&0&0&0&0&0\\
0&0&1&1&1&1&0&0&0&0&0&0&0&0&0&0&0&0\\
0&0&0&1&1&1&0&0&0&0&0&0&0&0&0&0&0&0\\
0&0&0&0&1&1&0&0&0&0&0&0&0&0&0&0&0&0\\
0&0&0&0&0&1&0&0&0&0&0&0&0&0&0&0&0&0\\
0&0&0&0&0&0&1&1&1&0&0&0&0&0&0&0&0&0\\
0&0&0&0&0&0&0&1&1&0&0&0&0&0&0&0&0&0\\
0&0&0&0&0&0&0&0&1&0&0&0&0&0&0&0&0&0\\
0&0&0&0&0&0&0&0&0&1&1&1&1&0&0&0&0&0\\
0&0&0&0&0&0&0&0&0&0&1&1&1&0&0&0&0&0\\
0&0&0&0&0&0&0&0&0&0&0&1&1&0&0&0&0&0\\
0&0&0&0&0&0&0&0&0&0&0&0&1&0&0&0&0&0\\
0&0&0&0&0&0&0&0&0&0&0&0&0&1&1&1&1&1\\
0&0&0&0&0&0&0&0&0&0&0&0&0&0&1&1&1&1\\
0&0&0&0&0&0&0&0&0&0&0&0&0&0&0&1&1&1\\
0&0&0&0&0&0&0&0&0&0&0&0&0&0&0&0&1&1\\
0&0&0&0&0&0&0&0&0&0&0&0&0&0&0&0&0&1
\end{bmatrix} \tag{13}$$

topology matrix [*TCM*] for the test network is shown in Equation (13). The boundary detection matrix [*BDM*] shows that the system is divided into four subsystems. The system with busbar (1) is not considered as an island as it is connected to the main grid.

$$[BDM]=\begin{bmatrix}
1&7&8&9&0\\
2&3&4&5&6\\
10&11&12&13&0\\
14&15&16&17&18
\end{bmatrix} \tag{14}$$

As shown in the results, the proposed method is capable of detecting the configuration of Islands in the distribution network. Moreover, the proposed method is capable of tracking any changes in the island configuration. If the island's configuration changed due to any reason such as faults in the system or self-healing strategies, the proposed method can detect the new configuration without applying any further modification.

6.2. Dynamic Voltage Sensitivity Factor

When intentional islanding event is initiated via opening the line sections L1, L9 and L13, the stable operation of each island should be assured. The remaining generation and load in each island should be balanced to avoid voltage collapse. A proposed dynamic voltage sensitivity factor is used to identify weak busbars in each island. In Island-2, total available generation is 2 MVA while Table (4) shows the load demand in Island-2 busbars.

Table 4: Load demand in island-2

Busbar	Active Power (MW)	Reactive Power (MVar)
Bus10	1.055	0.2842
bus11	0.5916	0.2615
Bus12	0.9267	0.2255
Bus13	0.9268	0.2278

Since Island-2 is not stable due to lack of generation, Island-2 was used to validate the proposed DVSF. The busbar voltages for Island-2 are shown in Figure 9. As shown, the busbar voltages collapsed after islanding. Similarly, generator angular velocity and system frequency as shown in

Preprints (www.preprints.org) | NOT PEER-REVIEWED | Posted: 9 May 2017 doi:10.20944/preprints201705.0082.v1

Figure 10(a) and 10(b) also collapses. Hence, it is vital to identify the unstable busbars to perform the wide area load shedding.

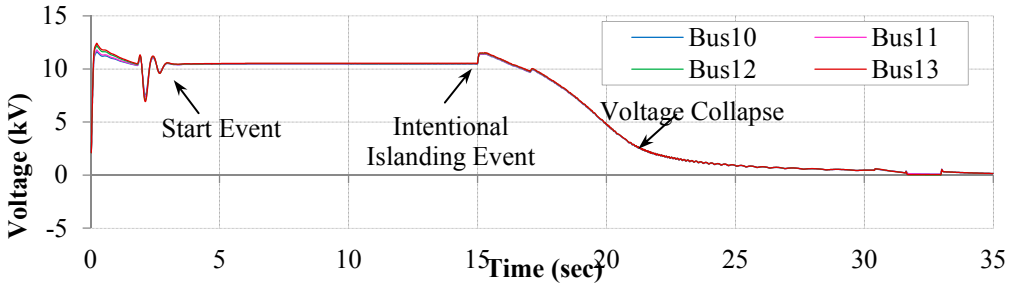

Figure 9. Voltage collapse in the island-2 after intentional islanding event.

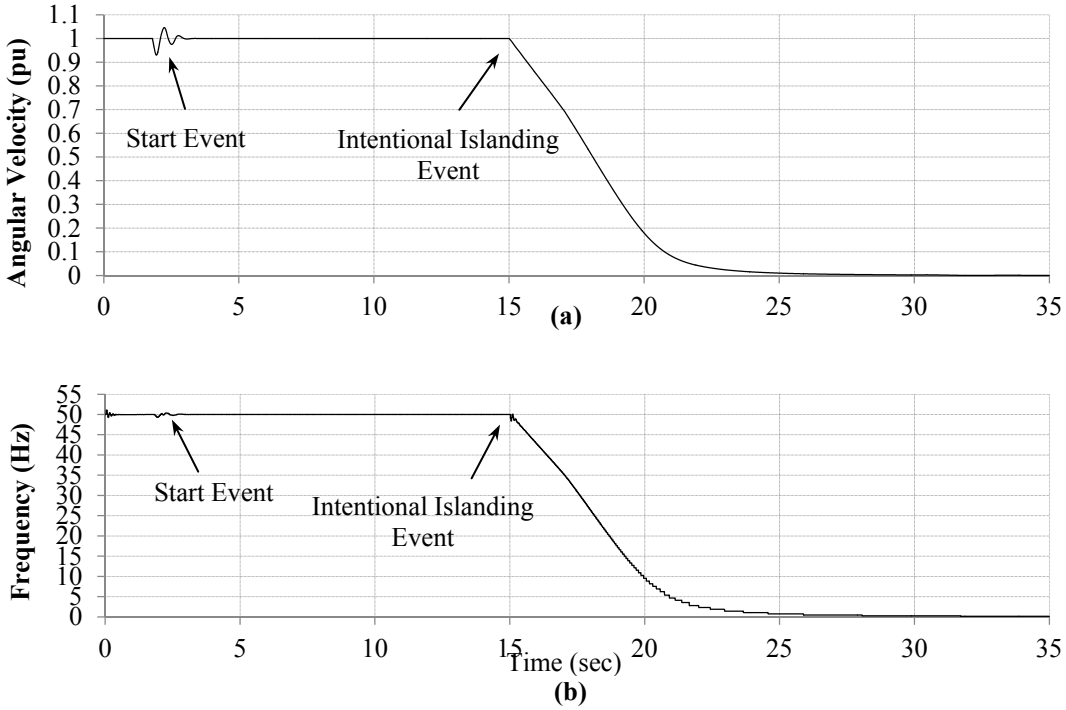

Figure10. System parameters (a) synchronous generator angular velocity, (b) island-2 frequency.

The full window of the calculated conventional voltage sensitivity index using pre-islanding data is shown in Figure 11(a) and the expanded window during the islanding is demonstrated in Figure 11(b). With reference to the results, the most stable busbar is Bus11, since it has the lowest sensitivity index and the most sensitive busbar is Bus13. Hence, according to results calculated using conventional method, load-shedding program should start with Bus13 by virtue of being the weakest busbar and proceed to Bus10, 12 and 11. However, in the proposed scheme, once islanding occurs, the new system topology is used to calculate the DVSF. The calculated DVSF for Island-2 is illustrated in Figure 12. The results in Figure 12 show that the Bus13 is still the weakest busbar followed by Bus 10, Bus 11 and Bus12.

Preprints (www.preprints.org) | NOT PEER-REVIEWED | Posted: 9 May 2017 doi:10.20944/preprints201705.0082.v1

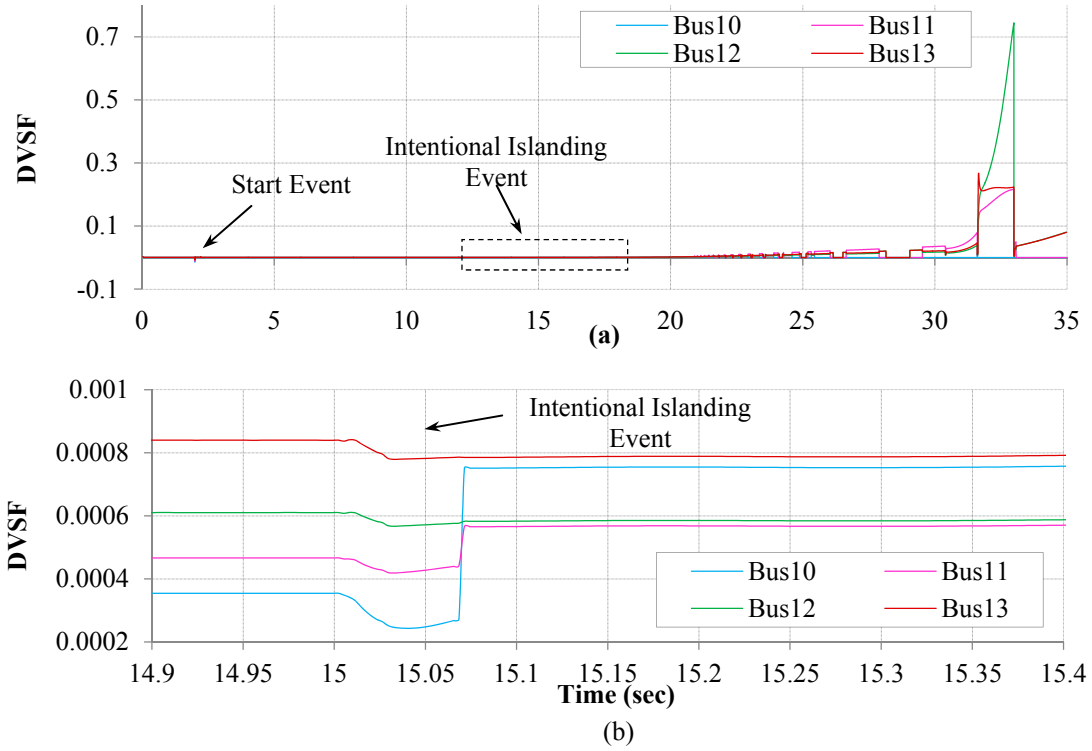

Figure 11. Dynamic Voltage Sensitivity Factor (a) full window of DVSF for busbars in the island-2 (b) Expanded window for DVSF during 'Intentional Islanding Event'

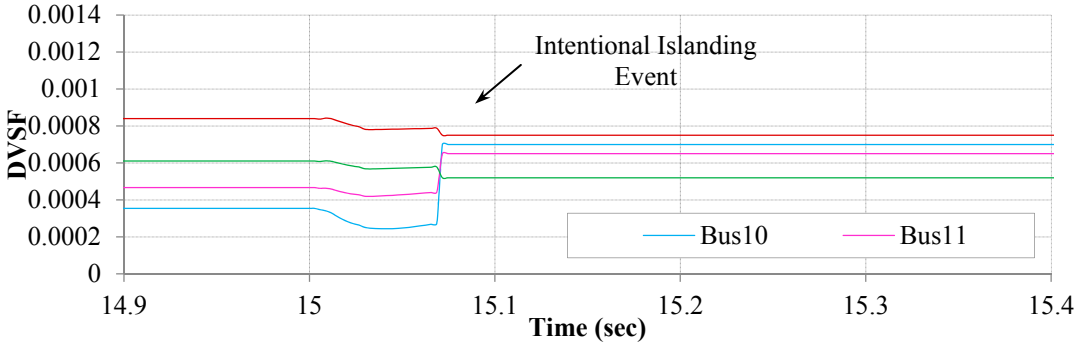

Figure 12. Voltage sensitivity indices using proposed boundary detection method.

6.3. Wide Area Load Shedding

In this section, Island-2 was used to verify the robustness of the proposed wide area load shedding to improve the voltage profile of the microgrid. Once the weak busbars were identified, the load shedding was performed to prevent voltage collapse. The amount of load shedding is related to the system frequency. Moreover, the DG unit should be able to work ±10% of its rated value for 20-30 minutes [32].

In order to control the voltage of the system, the power factor of the DG unit was varied between 0.85 lagging to 0.9 leading. According to the IEEE-Standard 1547, the system should be capable of operating for 300 sec when frequency deviation was less than ±5% of the rated value.

Based on Table (4), there are 1.82 MW excess load in island-2. Thus, according to the previous section, Bus13 as the weakest busbar and Bus10 as the second weakest busbar were chosen to perform the load shedding. The obtained results for the system parameters are shown in Figure 12 and 13. All the voltages of the busbars are illustrated in Figure 12. By comparing Figure 9 and Figure 13, it confirms that the proposed load shedding prevented voltage collapse in the system. As shown, all

Preprints (www.preprints.org) | NOT PEER-REVIEWED | Posted: 9 May 2017 doi:10.20944/preprints201705.0082.v1

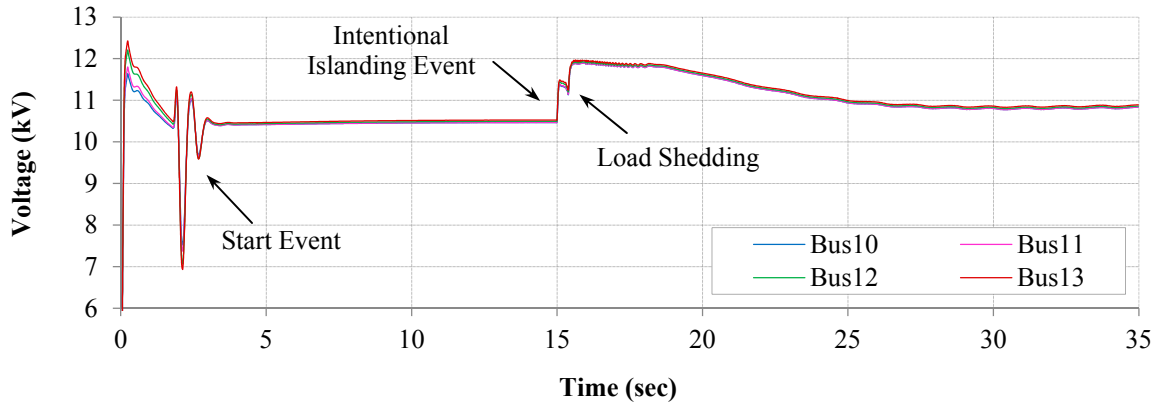

Figure 13. Voltage profile in island-2 recovers after load shedding.

the voltages are in the acceptable range. Synchronous generator speed and frequency of the system are shown in Figure 14.

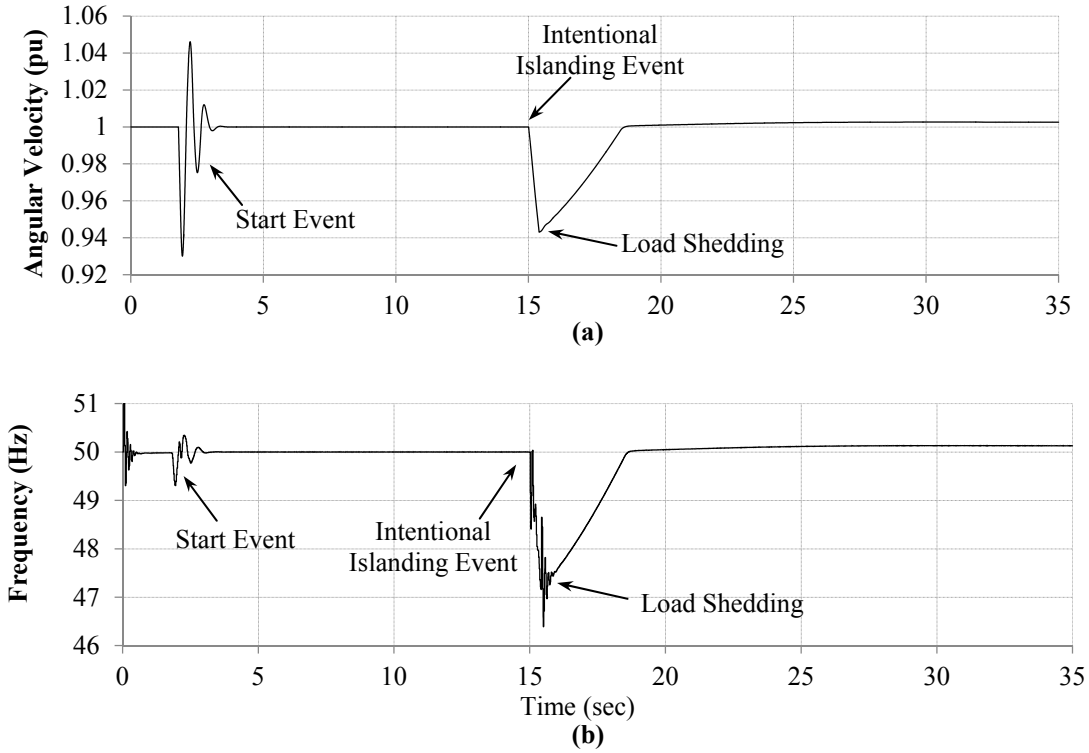

Figure14. System parameters (a) synchronous generator angular velocity, (b) island-2 frequency.

The speed of the generator was recovered after load shedding to 1 pu. Similarly, system frequency recovers to 50 Hz after the wide area load shedding. A full window of the dynamic voltage sensitivity factor is shown in Figure 15(a). An expanded window during 'intentional islanding event' and 'load shedding' is shown in Figure 15(b). As illustrated in Figure 15, the DVSF for all busbars remained near zero, which confirms the voltage stability in the Island-2.

It can be concluded from the results of this section, that the proposed load shedding represented a vast improvement to voltage stability by considering the dynamic performance of the system during the islanding operation for Island-2. Hence, the proposed boundary detection method and the corresponding load shedding have the ability to reconfigure the islands and improve the profile of the voltages in all busbars.

Preprints (www.preprints.org) | NOT PEER-REVIEWED | Posted: 9 May 2017 doi:10.20944/preprints201705.0082.v1

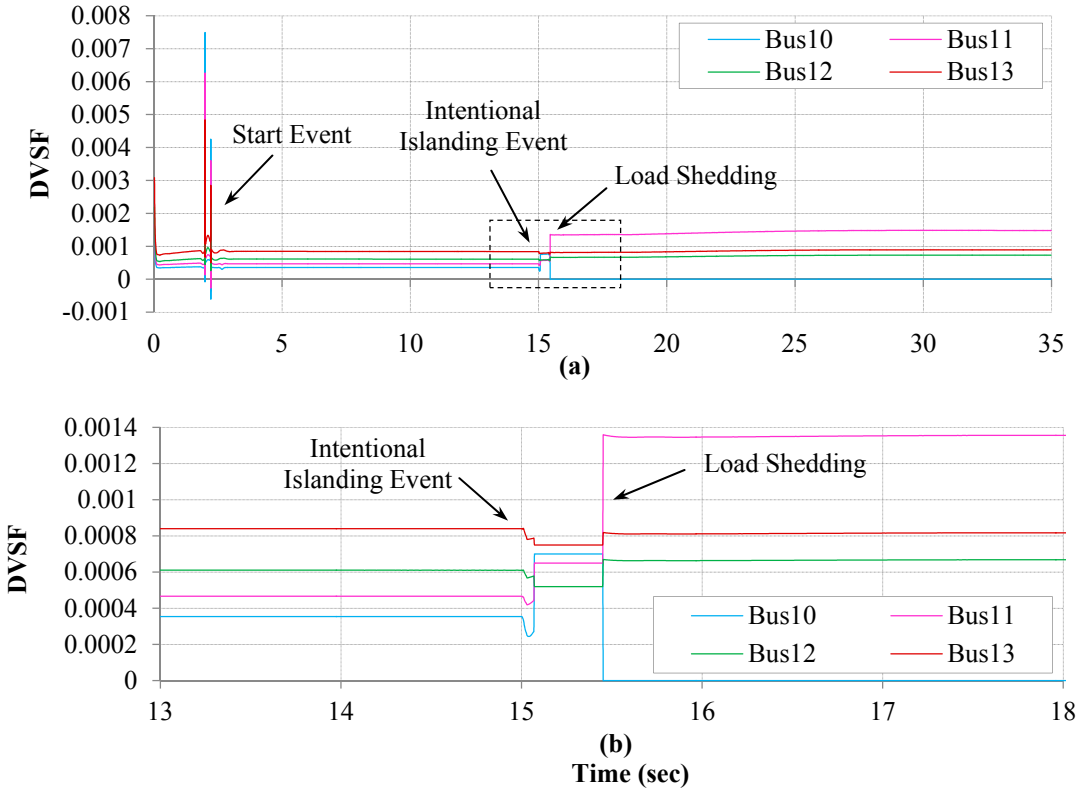

Figure 15. Dynamic voltage sensitivity factor (a) full window of DVSF for busbars in the island-2, (b) Expanded window for DVSF during 'intentional islanding event' and 'load shedding'

7. Conclusions

This paper presents a novel scheme to detect the configuration of islands in distribution systems. Moreover, the proposed scheme assures the stable operation of islands using wide area load shedding during autonomous mode. The results have shown that the proposed boundary detection method is capable of accurately identifying the system topology. Furthermore, the proposed dynamic sensitivity factor is calculated for all busbars of an island and the obtained results proved that using the DVSF reflects the system's dynamic performance and can be used to detect the weakest busbar in the system. Wide area load shedding was performed on weak busbars and the results confirmed the IEEE-1547 standard in terms of voltage and frequency of the island.

Acknowledgments: No funding resources

Author Contributions: For research articles with several authors, a short paragraph specifying their individual contributions must be provided. The following statements should be used "Aref Pouryekta, Vigna K. Ramachandaramurthy, Sanjeevikumar Padmanaban, as developed the original proposed research work and implemented with numerical simulation software for investigation and performance validation. c contributed his experience in boundary deduction issues in faulty condition for the proposal its verification of the obtained results based on theoretical concepts and insight background. All authors involved to articulate the research work for its final depiction as research paper".

Conflicts of Interest: The authors declare no conflict of interest.

References

[1] B. Yu, M. Matsui, and G. Yu, "A review of current anti-islanding methods for photovoltaic power system," Solar Energy, vol. 84, pp. 745-754, 5// 2010.

[2] Y. Zhihong, A. Kolwalkar, Y. Zhang, D. Pengwei, and R. Walling, "Evaluation of anti-islanding schemes based on nondetection zone concept," in Power Electronics Specialist Conference, 2003. PESC '03. 2003 IEEE 34th Annual, 2003, pp. 1735-1741 vol.4.

[3] F. Wang and Z. Mi, "Notice of Retraction Passive Islanding Detection Method for Grid Connected PV System," in Industrial and Information Systems, 2009. IIS'09. International Conference on, 2009, pp. 409-412.
[4] H. Zeineldin and J. L. Kirtley Jr, "A simple technique for islanding detection with negligible nondetection zone," Power Delivery, IEEE Transactions on, vol. 24, pp. 779-786, 2009.
[5] A. Khamis, H. Shareef, E. Bizkevelci, and T. Khatib, "A review of islanding detection techniques for renewable distributed generation systems," Renewable and Sustainable Energy Reviews, vol. 28, pp. 483-493, 2013.
[6] S. Syamsuddin, N. Rahim, and J. Selvaraj, "Implementation of TMS320F2812 in islanding detection for Photovoltaic Grid Connected Inverter," in 2009 International Conference for Technical Postgraduates (TECHPOS), 2009.
[7] N. Lidula and A. Rajapakse, "A pattern recognition approach for detecting power islands using transient signals—Part I: Design and implementation," Power Delivery, IEEE Transactions on, vol. 25, pp. 3070-3077, 2010.
[8] J. Laghari, H. Mokhlis, M. Karimi, A. Bakar, and H. Mohamad, "Computational Intelligence based techniques for islanding detection of distributed generation in distribution network: A review," Energy Conversion and Management, vol. 88, pp. 139-152, 2014.
[9] H. Zeineldin, E. F. El-Saadany, and M. Salama, "Impact of DG interface control on islanding detection and nondetection zones," Power Delivery, IEEE Transactions on, vol. 21, pp. 1515-1523, 2006.
[10] C. Li, C. Cao, Y. Cao, Y. Kuang, L. Zeng, and B. Fang, "A review of islanding detection methods for microgrid," Renewable and Sustainable Energy Reviews, vol. 35, pp. 211-220, 2014.
[11] S. Raza, H. Mokhlis, H. Arof, J. Laghari, and L. Wang, "Application of signal processing techniques for islanding detection of distributed generation in distribution network: A review," Energy Conversion and Management, vol. 96, pp. 613-624, 2015.
[12] M. Ropp, J. Ginn, J. Stevens, W. Bower, and S. Gonzalez, "Simulation and Experimental Study of the Impedance Detection Anti-Islanding Method in the Single-Inverter Case," in Photovoltaic Energy Conversion, Conference Record of the 2006 IEEE 4th World Conference on, 2006, pp. 2379-2382.
[13] P. O'Kane and B. Fox, "Loss of mains detection for embedded generation by system impedance monitoring," in Developments in Power System Protection, Sixth International Conference on (Conf. Publ. No. 434), 1997, pp. 95-98.
[14] H. Mohamad, H. Mokhlis, and H. W. Ping, "A review on islanding operation and control for distribution network connected with small hydro power plant," Renewable and Sustainable Energy Reviews, vol. 15, pp. 3952-3962, 2011.
[15] K. N. E. K. Ahmad, J. Selvaraj, and N. A. Rahim, "A review of the islanding detection methods in grid-connected PV inverters," Renewable and Sustainable Energy Reviews, vol. 21, pp. 756-766, 2013.
[16] A. Balaguer, x, I. J. lvarez, and E. I. Ortiz-Rivera, "Survey of Distributed Generation Islanding Detection Methods," Latin America Transactions, IEEE (Revista IEEE America Latina), vol. 8, pp. 565-570, 2010.
[17] M. Hanif, M. Basu, and K. Gaughan, "A discussion of anti-islanding protection schemes incorporated in a inverter based DG," in Environment and Electrical Engineering (EEEIC), 2011 10th International Conference on, 2011, pp. 1-5.
[18] M. Ropp, M. Begovic, and A. Rohatgi, "Analysis and performance assessment of the active frequency drift method of islanding prevention," Energy Conversion, IEEE Transactions on, vol. 14, pp. 810-816, 1999.
[19] B.-H. Kim, S.-K. Sul, and C.-H. Lim, "Anti-islanding detection method using Negative Sequence Voltage," in Power Electronics and Motion Control Conference (IPEMC), 2012 7th International, 2012, pp. 604-608.
[20] H. Karimi, A. Yazdani, and R. Iravani, "Negative-Sequence Current Injection for Fast Islanding Detection of a Distributed Resource Unit," Power Electronics, IEEE Transactions on, vol. 23, pp. 298-307, 2008.
[21] B. Bahrani, H. Karimi, and R. Iravani, "Nondetection Zone Assessment of an Active Islanding Detection Method and its Experimental Evaluation," Power Delivery, IEEE Transactions on, vol. 26, pp. 517-525, 2011.
[22] N. D. Tuyen and G. Fujita, "Negative-sequence Current Injection of Dispersed Generation for Islanding Detection and Unbalanced Fault Ride-through," in Universities' Power Engineering Conference (UPEC), Proceedings of 2011 46th International, 2011, pp. 1-6.
[23] L. Zhenzhi, X. Tao, Y. Yanzhu, Z. Ye, C. Lang, L. Yilu, et al., "Application of wide area measurement systems to islanding detection of bulk power systems," Power Systems, IEEE Transactions on, vol. 28, pp. 2006-2015, 2013.

[24] D. Lei, P. Zhencun, C. Wei, and P. Jianye, "An Integrated Automatic Control System for Distributed Generation Hierarchical Islanding," in Power System Technology, 2006. PowerCon 2006. International Conference on, 2006, pp. 1-6.

[25] L. Qin, F. Z. Peng, and I. J. Balaguer, "Islanding control of DG in microgrids," in Power Electronics and Motion Control Conference, 2009. IPEMC '09. IEEE 6th International, 2009, pp. 450-455.

[26] H. You, V. Vittal, and Y. Zhong, "Self-healing in power systems: an approach using islanding and rate of frequency decline-based load shedding," Power Systems, IEEE Transactions on, vol. 18, pp. 174-181, 2003.

[27] S. G. Zadeh, R. Madani, H. Seyedi, A. Mokari, and M. B. Zadeh, "New approaches to load shedding problem in islanding situation in distribution networks with distributed generation," 2012.

[28] R. A. Zahidi, I. Z. Abidin, H. Hashim, Y. R. Omar, N. Ahmad, and A. M. Ali, "Study of static voltage stability index as an indicator for Under Voltage Load Shedding schemes," in Energy and Environment, 2009. ICEE 2009. 3rd International Conference on, 2009, pp. 256-261.

[29] G. Wei, L. Wei, Z. Junpeng, Z. Bo, W. Zaijun, L. Zhao, et al., "Adaptive Decentralized Under-Frequency Load Shedding for Islanded Smart Distribution Networks," Sustainable Energy, IEEE Transactions on, vol. 5, pp. 886-895, 2014.

[30] J. Yin, L. Chang, and C. Diduch, "Recent developments in islanding detection for distributed power generation," in Power Engineering, 2004. LESCOPE-04. 2004 Large Engineering systems Conference on, 2004, pp. 124-128.

[31] W. Gao, "Comparison and review of islanding detection techniques for distributed energy resources," in 2008 40th North American power symposium, 2008, pp. 1-8.

[32] W. Xu, G. Zhang, C. Li, W. Wang, G. Wang, and J. Kliber, "A power line signaling based technique for anti-islanding protection of distributed generators—part i: scheme and analysis," Power Delivery, IEEE Transactions on, vol. 22, pp. 1758-1766, 2007.

[33] W. Wang, J. Kliber, G. Zhang, W. Xu, B. Howell, and T. Palladino, "A power line signaling based scheme for anti-islanding protection of distributed generators—Part II: field test results," Power Delivery, IEEE Transactions on, vol. 22, pp. 1767-1772, 2007.

[34] F. De Mango, M. Liserre, and A. D. Aquila, "Overview of anti-islanding algorithms for pv systems. part ii: Activemethods," in Power Electronics and Motion Control Conference, 2006. EPE-PEMC 2006. 12th International, 2006, pp. 1884-1889.

[35] D. Velasco, C. Trujillo, G. Garcerá, and E. Figueres, "Review of anti-islanding techniques in distributed generators," Renewable and sustainable energy reviews, vol. 14, pp. 1608-1614, 2010.

[36] L. Arya, S. Choube, and M. Shrivastava, "Technique for voltage stability assessment using newly developed line voltage stability index," Energy Conversion and Management, vol. 49, pp. 267-275, 2008.

[37] Y. Wang, W. Li, and J. Lu, "A new node voltage stability index based on local voltage phasors," Electric Power Systems Research, vol. 79, pp. 265-271, 2009.

[38] A. Sinha and D. Hazarika, "A comparative study of voltage stability indices in a power system," International journal of electrical power & energy systems, vol. 22, pp. 589-596, 2000.

[39] F. Shariatzadeh, C. B. Vellaithurai, S. S. Biswas, R. Zamora, and A. K. Srivastava, "Real-Time Implementation of Intelligent Reconfiguration Algorithm for Microgrid," Sustainable Energy, IEEE Transactions on, vol. 5, pp. 598-607, 2014.

[40] S. F. Alwash and V. K. Ramachandaramurthy, "DIRECT POWER FLOW METHOD FOR BALANCED AND UNBALANCED RADIAL DISTRIBUTION SYSTEMS WITH MULTI REFERENCE BUSES."

[41] P. Kundur, N. J. Balu, and M. G. Lauby, Power system stability and control vol. 7: McGraw-hill New York, 1994.